CONF-850716--4

BASIC ASPECTS OF ION BEAM MIXING*

CONF-850716--4

DE85 018391

R. S. Averback
Materials Science and Technology Division
Argonne National Laboratory
Argonne, Illinois 60439

July 1985

Invited paper presented at the 7th International Conference on Ion Beam Analysis, July 8-12, 1985, Berlin. To be published in the Journal of Nuclear Instruments and Methods.
*Work supported by the U. S. Department of Energy.

BASIC ASPECTS OF ION BEAM MIXING*

R. S. Averback
Materials Science and Technology Division
Argonne National Laboratory
Argonne, Illinois 60439

July 1985

Invited paper presented at the 7th International Conference on Ion Beam Analysis, July 8-12, 1985, Berlin. To be published in the Journal of Nuclear Instruments and Methods.
*Work supported by the U. S. Department of Energy.

BASIC ASPECTS OF ION BEAM MIXING*

R. S. Averback
Materials Science and Technology Division
Argonne National Laboratory
Argonne, Illinois 60439

Irradiation of solids with energetic particles results in the reorganization of constituent target atoms, i.e., ion beam mixing (IM). At low temperatures, IM is characterized by prompt (10^{-10}s) diffusion processes which are localized in the vicinity of the displacement cascade. Mixing at low temperatures can cause the system to depart far from the equilibrium state. At elevated temperatures, the diffusion of radiation-induced defects extends the mixing to longer times and greater distances. These delayed IM processes tend to return the system toward equilibrium. Recent experimental progress has led to a qualitative understanding of the fundamental aspects of IM in both temperature regimes. This has been achieved through systematic measurements of the influences of temperature, dose, dose-rate, cascade energy density, and chemical interactions on IM. The results of these experiments will be reviewed and compared to IM models based on collisional, thermal spike, and radiation-enhanced diffusion processes. The relation of IM to other fundamental radiation damage effects will also be discussed.

*Work supported by the U. S. Department of Energy.

FUNDAMENTAL ASPECTS OF ION BEAM MIXING

by
R.S. Averback
Argonne National Laboratory
Argonne, IL 60439

1 INTRODUCTION

Irradiation of a solid with energetic particles can lead to the displacement of many target atoms away from their initial lattice sites. This process, often referred to as ion beam mixing (IM), has been vigorously studied since ~1979. Part of the enthusiasm for IM has, of course, been spawned by the expectation that it could find technical significance as a method of materials modification. IM has also been of interest in the basic research community as it has raised many questions regarding atomic displacement and diffusion processes in irradiated materials. There have been several recent review articles on this topic (1-5) and these have been very useful in tabulating the results of both experimental and theoretical investigations; they also have established general trends for IM. Most of these reviews, however, have treated IM as a new phenomenon rather than a manifestation of fundamental displacement processes in irradiated materials. Consequently, the insight garnered from many years of radiation damage research has often been overlooked despite its obvious implications for the understanding of IM. In this article, therefore, an attempt will be made to evaluate the present understanding of IM in view of progress made in both basic IM and radiation damage research.

2 DISPLACEMENT PROCESSES

2.1 CASCADE EVOLUTION

The combination of binary collision and molecular dynamics computer simulations (BC and MD, respectively) have provided a detailed picture of the atomic displace-

ment process in irradiated materials. BC simulations have revealed that as an energetic atom comes to rest within a solid, it makes a series of collisions with target atoms. For sufficiently high incident particle energies, the distance between primary recoils, above some keV, is large, and each primary recoil can be considered to initiate an independent subcascade. This picture is represented in Fig. 1 where the primary recoils along a simulated 100-keV Fe ion trajectory in Fe are schematically illustrated (6). Within each subcascade, some of the target atoms receive sufficient energy to be ejected from their lattice sites, and these secondary recoil atoms produce yet additional secondary recoils. When energies fall below a few hundred eV, the approximation of binary collisions begins to break down, as many body collisions become important, and molecular dynamics simulation calculations must be employed. MD simulations, which were pioneered by Vineyard et al. at Brookhaven (7), reveal that at low energies the atomic displacements occur by replacement collision sequences (RCSs) in which one atom replaces its neighbor rather than atoms recoiling far from their initial lattice sites. Experimental evidence suggests that RCSs propagate, on the average, only a few atomic distances in cascades, although in some special cases, "focussed" RCSs can result in rather long chains (8). The initial knock-on site in such a sequence is left as a vacancy. Since the energy distribution of secondary recoils is strongly weighted toward low energies, approximately as $1/E^2$ (9), most atomic displacements are produced by RCSs rather than by high energy recoil atoms. As energies fall below a few eV, no additional point defects can be created. At this point, the lattice is highly disorganized by the large concentration of defects, often several percent. In addition, the region in the vicinity of the primary recoil event becomes highly excited as the initial recoil energy is partitioned among all atoms in the cascade. The large strain and residual agitation of the lattice leads to a final relaxation phase of the cascade. This phase of the cascade involves many body interactions. MD simulations show that within $\simeq 1 \times 10^{-12}$ s, close self-interstitial atom:vacancy pairs, i.e. Frenkel pairs (FPs), spontaneously recombine (7,10,11). In the

next $\simeq 10^{-11}$ s, the agitation of the lattice stimulates the motion of both vacancies and interstitials. This leads to a diffusive motion, or mixing; it also reduces the number of FPs by additional recombination reactions. Figure 2 illustrates the time development of a small cascade in W (2.5 keV) as simulated by MD (11). In the early phases of the cascade, the number of FPs rapidly increases. Then, spontaneous recombination becomes important and the number of FPs diminishes. At the end of this second phase, the number of FPs agrees well with predictions of BC calculations yielding the so called "Kinchin-Pease" number (see below). Finally, the FP number is further reduced, by about a third, by the stimulated diffusive motion of the remaining point defects. This phase of the cascade is often referred to as a thermal spike. MD simulations have shown, in fact, that in this latter part of the cascade, the energy becomes equally divided into kinetic and potential components, indicating local equilibrium (10).

From the above picture, it can be seen that complete characterization of IM requires full MD simulations. These calculations, however, are presently limited to a few keV in energy, and for the most part, to pure metals. The qualitative findings of low energy MD simulations suggest, however, that a heterogeneous cascade model for IM can be constructed by dividing the cascade evolution into three distinct phases, displacement, spontaneous relaxation, and thermal spike phases. Thus, the contribution of each of these phases to IM will be separately considered.

2.2 DISPLACEMENT PHASE

The displacement phase is characterized by a small number of high energy primary recoils and the production of many FPs by low-energy secondary recoils. This phase of the cascade is reasonably approximated by BC models, except, perhaps, for the production of focussed RCSs. Two methods are available for BC calculations, Monte Carlo type computer simulations and analytical transport theory. Simulation programs were initially developed for defect production studies (12,13). These programs follow all

atoms which have energies greater than some cutoff energy, usually taken to be about 5 eV (even though MD is necessary at this low energy). The position of each self-interstitial atom and its associated vacancy is retained. When all atoms fall below the threshold energy, the displacement phase is terminated. Not all of the Frenkel pairs generated by this method are stable. Therefore, a spontaneous recombination volume, deduced from either simulation (7) or radiation annealing experiments (14), is drawn around each vacancy in which self-interstitials are unstable to recombination. In this way, point defect production as a function of energy can be calculated. The results of these calculations are that FP production is rather well described by the modified Kinchin-Pease model; i.e.

$$\upsilon = \begin{cases} 0 & T<E_d \\ 1 & E_d<T<2.5\ E_d \\ 0.8E_D/2E_d & 2.5E_d<T \end{cases} \qquad (1)$$

where E_D is the damage energy, and E_d is the displacement energy. Similar results were obtained by analytical models based on linearized transport theory (15). In these calculations, spontaneous recombination is artificially included by use of the displacement threshold E_d.

Both analytical (16-18) and simulation BC (19,20) models have also been employed to study IM. Recently, Eckstein and Möller (19) modified the simulation program, TRIM (21), to calculate IM. TRIM assumes that the target is amorphous and therefore neglects any displacement mechanisms involving crystalline effects. The modified program, TRIDYN, retains the location of specific marked atoms. Unlike the defect production calculations, however, many trajectories are followed to obtain the mixing for one case history, and therefore, the lattice is allowed to relax to a uniform density after each trajectory. In principle, simulations seem more straight-forward than analytical approaches. However, two important assumptions in the simulations, as in the analytical models, are that recoiling atoms only collide with stationary atoms, i.e. linear

cascades, and that the details of processes involving low energy recoils (below 50 eV) can be neglected. The success of the model, therefore, depends on the characteristic energy of the process of interest. Atomic motion within a thermal spike, for example, has no meaning within this model.

Below ~1000 eV, the BC approximation begins to break down as many body interactions become important. MD simulations show that RCSs become the dominant mode of atomic transport. These simulations are also able to follow atomic rearrangement during spontaneous relaxation, i.e., point defect recombination and agglomeration. No model other than MD adequately describes this phase. An estimate of IM in this phase can be obtained by assuming that unstable interstitials follow different recombination paths from their production paths. Assuming further that they are more numerous in number than stable interstitials, but are closer to their vacancies, suggests that diffusion by spontaneous relaxation should be similar or perhaps smaller in magnitude than that in the displacement phase.

2.3 THERMAL SPIKES

One picture of cascades, suggested in 1956 by Seitz and Koehler (22) is that they are local "hot spots" in the lattice. Recently, Peak and Averback (PA) have calculated the effect of such thermal spikes on point defect production and IM (23). Using the MD simulations as a guide, PA assume that FPs are produced in the cascade region during the displacement phase of the cascade, and that these point defects then diffuse during the subsequent thermal spike. Results of BC calculations are employed to establish the initial conditions of the spike. Analytical models are simplest for this purpose as they yield average parameters. Since analytical models do not explicitly include subcascade formation, PA assume that each primary recoil atom initiates an independent subcascade as suggested by Fig. 1. The damage energy and volume of each subcascade is taken from the tables of Winterbon (24). Using the expression $3kT=E_D/n_o$ (n_o is the atomic

concentration) and the Kinchin-Pease expression, the initial cascade temperature and FP concentration are determined. Evolution of the heat and FP distributions are then calculated using heat flow and chemical rate theory equations, respectively. The total self-diffusion coefficient is taken to be, (25)

$$D = D_i c_i + D_v c_v, \tag{2}$$

where,

$$D_i = D_{oi} \cdot \exp(\Delta H_{mi}/kT), \text{ and } D_v = D_{ov} \cdot \exp(\Delta H_{mv}/kT),$$

ΔH_{mi} and ΔH_{mv} are self-interstitial and vacancy migration enthalpies, respectively, and D_{oi} and D_{ov} are the corresponding prefactors. The cascade is assumed to quench at a time 1×10^{-11} s., the characteristic time for transferring energy from the phonon to electronic systems. If the heat dissipates more quickly by lattice heat conduction, diffusion automatically stops since the diffusion coefficient becomes small. For the case of bilayer samples, when chemical interactions can play a role, the effective diffusion coefficient is modified, as originally suggested by Johnson et al. (4), by adding the so-called Darken term,

$$D^* = D_{AB} \cdot (1 - 2\Delta H/kT) \tag{3}$$

where ΔH is the heat of mixing, and D_{AB} is the effective interdiffusion coefficient for the binary system. In the regular solution model, ΔH is given by,

$$\Delta H = \omega \cdot c(1 - c) \tag{4}$$

and ω is defined as $\omega = \omega_{AB} - (\omega_{AA} + \omega_{BB})/2$, and the ω_{ij} are the interaction energies between i and j atoms; c is the concentration of B atoms. For atomic species which are strongly attracted, i.e. negative heat of mixing, the diffusion is biased toward interdiffusion. On the other hand, for positive heats of mixing, the different atomic species tend to segregate.

2.4 RADIATION-ENHANCED DIFFUSION

The diffusive processes which occur after the cascade region comes to equilibrium with the lattice, i.e. RED, depends strongly on defect mobilities, point defect concentrations and the instantaneous defect structure of the sample, and these are all functions of the specimen temperature (25). RED has been studied many years and it is beyond the scope of this article to discuss it in detail. However, in evaluating the influence of RED on IM, it is illuminative to divide the temperature scale according to the well known annealing stages I, III, and V (26). In stages I and III, self interstitials and vacancies become mobile, respectively. In stage V, point defect clusters and dislocation loops dissolve by thermal diffusion of vacancies. By examining the temperature dependence of mixing in terms of these characteristic temperatures, insight regarding the diffusion process can be gleaned.

3 EXPERIMENTAL OBSERVATIONS

3.1 DEFECT PRODUCTION

It has been known for some years now that the Kinchin-Pease expression overestimates the number of FPs produced in energetic cascades by a factor of ~3. In Fig. 3, the ratio of the number of FPs produced in cascades, deduced from electrical resistivity measurements of ion-irradiated Cu thin films, to that obtained from the Kinchin-Pease expression, is plotted as a function of cascade energy (27). This ratio is

denoted as the defect production "efficiency" ξ. The energy scale is in the dimensionless units of $T_{1/2}/E_d$. $T_{1/2}$ is the energy of the average subcascade of an irradiation and is a useful parameter to characterize the primary recoil spectrum of an irradiation (27). Systematic studies in Al (28), Ag (27), and Fe (29) and less systematic studies of several other metals have all shown similar results with no exceptions (30). The results of BC and MD simulations are also plotted in the figure. For the BC simulations, the efficiency varies little with energy. These results demonstrate that the approximation of binary collisions is incomplete in describing displacement processes. It is unsurprising, therefore, that they should have similar deficiencies in describing IM. The results of MD for defect production in W are also shown in Fig. 3 (11). An excellent correlation with experimental results is obtained. The highest cascade energy in the simulation is 10 keV. At this cascade energy, the efficiency in the simulations appears to be leveling off, similar to the experiments, and branching or subcascade formation begins to occur (31).

The two important features of this experiment in regards to IM, are: 1) The defect production efficiency decreases almost precisely as predicted by MD calculations providing strong evidence for point defect diffusion in the thermal spike portion of the cascade. In this regard, PA also found good agreement with the resistivity results for Cu in Fig. 3, as well as for Al and Ag, using their thermal spike model. (2) The efficiency becomes constant above 5-10 keV due to subcascade formation. The second conclusion is predicted by BC simulations (6) and is observed in field-ion microscope studies of cascade structures in W and Pt (32). This result is important as it indicates that the substructure of cascades, more than average total cascade parameters, determines point defect production and IM.

3.2 DISORDERING

Although defect production studies have been very useful in elucidating displacement processes in cascades, particularly in conjunction with MD simulations,

they do not provide a quantitative measure of atomic diffusion which is necessary for understanding IM. More direct measurements of diffusion are measurements of the rate of disordering during irradiation of initially ordered alloys. Using the MD result that nearly all displacements of atoms in a cascade occur by displacements of 1 atomic distance, i.e., a replacement collision sequence or a point defect diffusion step, disordering can be modeled on the basis of the number of random replacement jumps. In this way the number of replacements per "Kinchin-Pease displacement" can be extracted from disordering experiments. Table 1 is a partial compilation of disordering results for irradiations performed at low temperatures. The tabulated results clearly illustrate the large number of replacements per displacement for cascade producing irradiation. For electron irradiation, for which recoil energies are mostly below 100 eV, the number of replacements per displacement is small, and close to the values expected for the displacement phase. Other measurements of the critical dose to disorder an alloy are consistent with these measurements, i.e., the dose required for cascade producing irradiation to disorder an alloy is an order of magnitude smaller than that for electron damage (33). Again, the point is that in cascades, the agitation of the lattice stimulates much point defect motion. As atom energies in the cascade are high relative to ordering energies, the diffusion tends to disorder the alloy. An alternate hypothesis for the disordering is that it is due to RCSs, and that these sequences are longer for cascades than electron irradiation. This point will be discussed below in regards to IM.

3.3 VACANCY CLUSTERING

A final measurement illustrating atomic diffusion in cascades, which can only be explained by relaxation processes, is the agglomeration of vacancies in cascade regions. Electron microscopy observations of Mo, for example, irradiated at temperatures where vacancies are immobile, first revealed vacancy-type dislocation loops associated with individual cascades (34). Similar results were recently found for Ag (35), Au (36), and

Cu_3Au (37); the irradiations and observations for these three cases were performed near 10 K. In W, three dimensional void-like agglomerates were observed by field-ion microscopy after W_2 or Ag_2 molecule irradiation at 10 K (38). These observations demonstrate that vacancy motion must take place during the cascade lifetime.

4 EXPERIMENTAL OBSERVATIONS - IM

4.1 EXPERIMENTAL CONSIDERATIONS

Two geometries have been employed for basic diffusion studies of IM, the marker and bilayer geometries. Markers provide the simpler geometry for extracting diffusion data. Typically, these specimens are fabricated by vapor depositing material A onto some substrate, then depositing about 5-30 Å of material B, followed by another layer, 300-500 Å, of A. Bilayer samples are prepared by depositing one layer onto a substrate followed by deposition of the second layer. In some cases, the substrate is employed as the first layer although this procedure seems prone to contamination unless the substrate can be well cleaned in situ. Before describing the results of experiments, it seems appropriate to briefly discuss the experimental problems associated with each geometry to provide some intuition regarding the accuracy and reproducibility of reported results. It is assumed that during the mixing experiment the marker becomes dilute quickly and that no chemical interactions are important. For systems which have large mutual solubilities or form compound phases, this assumption seems reasonable. In cases were there is no solubility, it is possible that the marker initially "balls up" upon deposition, creating a bilayer type geometry. "Balling-up" may also occur upon irradiation, as was suggested by Westendorp et al. (39). Another experimental problem with markers is contamination as the marker is bounded by two interfaces. Since a relatively small number of atoms are involved in the marker, a few monolayers of oxygen, for example, can react with all the marker atoms. Indeed, reproducibility of results has been a non-trivial problem which has plagued the evaluation of marker experiments.

Bilayer geometries pose more severe problems with analysis. Generally, unfolding the resolution in the backscattering system is more difficult. More importantly, a) mixing occurs at all compositions, and b) the damage profile is non-uniform across the mixed region. These two effects require a more detailed analysis of the data, such as using a Boltzmann-Matano type of analysis. It also requires very accurate determinations of the damage distribution. Bilayers have the advantage, however, that chemical effects can be studied. Moreover, this geometry is more relevant to materials modification problems.

4.2 IM DISTRIBUTIONS

At low temperatures in metals, the mixing profiles in marker and bilayer specimens can usually be described by Gaussian and complementary error (erfc) functions, respectively. Superposed onto the distribution for bilayer samples is a long tail of the top component into the substrate material; it contains a relatively small fraction of the mixed atoms (40). This component is due to implantation of primary recoil atoms. Both analytical (16) and Monte Carlo simulations (20) show good agreement with experiment. It is somewhat surprising that the profiles for bilayer samples fit the solution to the diffusion equation for the case of a concentration independent diffusion coefficient. Since for most bilayer systems investigated, the damage energy (see below) is considerably larger for the species having greater atomic number, some dependence on composition seems inevitable. Deviations resulting from such asymmetry are apparently not resolved in the data and perhaps are an indication of the accuracy of bilayer experiments.

In many silicides and some metals, it has been observed that mixed layers grow at room temperature, or above, with nearly constant composition (1). A comparison of the mixing distribution in Ni-Si with that in Ni-Al revealed that even when the irradiation and analyses were performed below 10 K, there was a strong tendency to

maintain constant composition in the silicide (41). Such stoichiometric growth has also been observed in a Au-Ge bilayer sample which had been irradiated (with Xe) and analyzed near 4 K (42). Unfortunately, defect properties in silicides or germanides are not well known, and therefore, one can only guess about the cause of stoichiometric growth. The simplest explanation would entail radiation-enhanced diffusion, although such an explanation for irradiations below 10 K is certainly tenuous as point defect motion at such low temperatures is very uncommon.

4.3 DOSE DEPENDENCE

Two components of IM have been resolved in bilayer experiments. The smaller component, as mentioned above, results from recoil implantation. The number of recoil atoms implanted by this mechanism increases linearly with dose as predicted by BC models. The larger component, which is described by the erfc function, broadens as the square root of dose. Similarly for marker specimens, the variance of the Gaussian distribution broadens as the square root of dose. A square root of dose dependence is predicted by all models involving stochastic processes.

For a few silicide systems, e.g. Cr, Au, V, and Pd silicides, linear growth kinetics were reported for room temperature irradiations (43). For Au-Si, linear growth was also observed at 80 K (44). In all of these examples, the distribution was stoichiometric. The combined results for these silicides, stoichiometric growth and a linear dose dependence, suggest that the mixing is not diffusion controlled but rather interface controlled. In Cr-Si, it was in fact shown using low energy irradiations, that irradiating only the Cr-$CrSi_2$ interface above 150°C led to continued growth of $CrSi_2$, but that irradiating only the Si-$CrSi_2$ interface did not (45). There have been no cases of linear growth kinetics reported for marker specimens, metal systems, or systems irradiated near 4 K.

4.4 SCALING WITH DAMAGE ENERGY

There are only a few systematic investigations of scaling of IM with damage energy. Matteson et al. first reported approximate scaling for markers in Si (46). Nicolet et al. also reported that IM scales reasonably well with damage energy for 80 K irradiations of Al, Si, Al_2O_3, and SiO_2 (2). Scaling with damage energy was also reported for low-temperature (80 K) irradiations of Cu using 0.5 and 1.8 MeV Kr ions (47). For all of these irradiations, scaling with damage energy is readily understood in terms of Fig. 1. For the Al and Si targets, the target masses are light and subcascade formation is expected for all the irradiations. For the Cu specimens, the Kr energies were sufficiently high that subcascade formation was again expected, even though Cu and Kr are relatively high in mass. It was noted in the Cu study that the primary recoil spectra for the 0.5 and 1.8 MeV Kr irradiations were very similar. It may seem that the Cu results are inconsistent with thermal spike models as the energy density for the higher energy irradiation, calculated by analytical theories, is smaller (24). This would imply that the spike temperatures are lower and, accordingly, that IM should be less. Rather, it illustrates that for high energy irradiations, average damage profiles obtained by transport equations are not appropriate for IM calculations and that it is the cascade substructure, i.e. subcascades, that is important.

In studies where the energy densities were varied over larger ranges, IM scaled less well with damage energy. Figure 4 illustrates IM in a bilayer Pt-Si (48) and a marker Ni(Au) (49) system. For both systems, IM per unit damage energy increases with increasing projectile mass. This behavior is reminiscent of that for point defect production efficiency shown in Fig. 3. Although this dependence of IM on energy density, like defect production, has no interpretation within BC models, it finds a natural interpretation within the thermal spike model. The light ion irradiations produce subcascades with very low recoil energies. For example, for the 300 keV He irradiation of Pt, only 25% of the damage energy is deposited in recoils above 6 keV. Low energy

subcascades are very inefficient in producing IM as they remain "hot" only very short times (50). For the heavy projectiles, Kr in Pt or Xe in Ni, the recoils have higher energy. Moreover, the distance between recoils becomes small and subcascade overlap can occur. This can lead to high energy densities and efficient mixing (23). Enhanced defect production (38) and sputtering (51) have previously been observed for cases of very high energy densities, i.e., nonlinear cascades.

4.5 MAGNITUDE OF IM

In comparing IM with other radiation effects, it is illuminative to consider the magnitude of IM. For this purpose the results for IM in a pure Cu bilayer (^{63}Cu-^{65}Cu) sample (52), irradiated at 6 K, are discussed. This reference example prevents any effects of chemical interactions or RED. Recoil implantation, as it is small and, in any case, well understood, will not be discussed further. A convenient measure of the magnitude of IM is the quantity, $Dt/\phi F_D$. The product Dt is obtained by fitting the experimental marker or interdiffusion profiles to the solution of the appropriate diffusion equation; ϕ is the ion dose; and F_D is the deposited damage energy per unit length normal to the surface. In as much as IM scales with damage energy (Sec. 4.4), and the width of the profile broadens as the square root of dose (Sec. 4.3), the ratio $Dt/\phi F_D$ is a normalized quantity independent of dose and the type of irradiation. For pure Cu, $Dt/\phi F_D = 20$ Å^5/eV. This value can be related to other radiation effects by casting it into the form of atomic jumps (or replacements) per atomic displacement. Using the expressions

$$Dt = 1/6 \cdot (vt) \cdot \lambda^2,$$

$$N' = 0.8E'_D/2E_d,$$

and

$$R' = \alpha N' = vt;$$

where υ is the atomic jump frequency, λ is the jump distance (interatomic spacing), N' is the displacements per atom, E'_D is the damage energy per atom, R' is the number of replacements per atom, and α is the number of replacements per displacement. Combining these equations, one obtains,

$$Dt/\Phi F_D = 0.067 \cdot \alpha \cdot \lambda^2/n_o \cdot E_d. \quad (5)$$

Substituting appropriate values for Cu in Eq. (5) yields $\alpha \simeq 100$ replacements per displacement. This value is an upper limit as some atoms will be transported more than 1 atomic distance. Nevertheless, the value for α obtained by IM compares rather well with that determined by disordering experiments in Cu_3Au (see Table 1). It is noteworthy that doses employed for disordering experiment are more than four orders of magnitude lower than those used for IM, yet similar results are obtained.

Littmark calculated IM in Cu using analytical transport theory (17). His results for a 200-keV Xe irradiation are $Dt/\Phi \cdot F_D \simeq 1$ Å^5/eV, which is much smaller than experiment. We note that this result corresponds to 5 replacements per displacement which is quite reasonable for displacement processes. Möller and Eckstein obtained $Dt/\Phi \cdot F_D \simeq 6$ Å^5/eV using TRIDYN for a 150 keV Ar irradiation of Fe (19). As this simulation considers only kinematics, results for Cu should be similar to Fe.

4.6 DEPENDENCE ON TARGET PROPERTIES

4.6.1 Physical Properties

To this point, there has been no consideration of the physical properties of the target other than through the damage energy calculation and the value of E_d. Recently, Kim et al. have investigated marker broadening in a large number of metal systems at low temperatures (53). The results of this work are summarized in Fig. 5. The data are

plotted to explicitly show the dependence of IM on two target parameters, the nuclear stopping power, F_D, (which is related to the atomic mass) and the cohesive energy. The data shown represent average values of IM for more than one type of marker in each target. It is clear from the figure that for fixed cohesive energy IM increases with increasing F_D (target mass), and for fixed F_D (atomic mass) it increases with decreasing cohesive energy. Moreover, these dependences are not weak, varying over an order of magnitude between IM in Au and Ti. The effect of cohesive energy was also investigated by Van Rossum et al. in very high mass bilayer systems (54). They also observed order of magnitude differences in IM between Au-Ag and W-Mo.

Interpretation of these data within analytical or simulation BC models is not easily possible. The target mass, for example, plays only a minor role in BC theories, and would presumably, in any case, predict a decrease in mixing with target mass. This can be seen by using the analytical expression for collisional mixing, (55)

$$Dt = 0.42 \cdot \phi F_D \cdot \langle R^2 \rangle / E_d \qquad (6)$$

where $\langle R \rangle$ is the range of a recoil with energy E_d, and E_d is the minimum displacement energy. The target dependent parameter is $\langle R^2 \rangle / E_d$, and since the range of recoils for fixed energy decreases with increasing target mass, it is expected that $\langle R^2 \rangle / E_d$ would similarly decrease. The cohesive energy may have some role in BC models as it is not unlikely that E_d is related to E_C.

The dependence of IM on target mass and cohesive energy can be readily understood within a thermal spike model on a qualitative basis. The mass of the target is important as it determines the energy density in the cascades, and energy density determines the cascade temperature. Noting Eq. (2), it can be seen that the higher the cascade temperature, the higher are the point defect diffusivities. The cohesive energy is also important for determining diffusion in the cascades, as the concentration of point

defects produced in the cascade tends to scale, although not exactly, with cohesive energy (56). The cohesive energy may also be important for diffusion in cascades since vacancy migration enthalpies scale with cohesive energy (57). This latter supposition implies that the vacancy diffusivity, D_v, is as important as the interstitial diffusivity, D_i, even though in thermal equilibrium, self-interstitial atoms have much higher diffusivities than vacancies. This possibility seems reasonable, however, for several reasons. First, Finis (58) has shown by MD that the vacancy migration enthalpy decreases dramatically in a cascade due to the very high vacancy concentration. Second, the observations noted above that vacancies agglomerate in cascades at temperatures well below stage III, indicate that vacancies are very mobile in cascades. Third, the MD simulations for W, Fig. 2, show that even for small, 2.5 keV, cascades, vacancies make nearly as many jumps as self-interstitials. Finally we note that the migration of self interstitial atoms at low temperatures involves a complicated interstitiacy mechanism which may not apply in cascades where the defect concentrations are very high, nor for interstitial impurities, which, of course, the markers are. Johnson et al. have suggested that the scaling of IM with cohesive energy is a consequence of the scaling of liquid diffusion with the cohesive energy (4). This opinion, however, assumes that the cascade can be considered as molten.

Calculations of IM using the thermal spike model have been made for the same systems as those shown in Fig. 5 (59). For the calculation, it was assumed, on the basis of the above discussion, that self-interstitials are immobile and that vacancies have an effective migration enthalpy in cascades equal to one third their migration enthalpy under thermal equilibrium conditions. The results are tabulated in Table 2. The agreement with experiment is exceptionally good. It should be noted that the calculation is symmetric in regards to the moving defect, and a mobile interstitial and immobile vacancy would yield the same results if the diffusivities were chosen similarly. The diffusion coefficients used in the calculation were derived from tracer impurity thermal diffusion data. This suggests that there may be a correlation between the thermal

diffusion and IM for different markers in a given host. There is not sufficient data in metal marker systems to test this idea, although Barcz et al. noted that the mixing of W, Pt, and Au markers in Si did scale with their respective thermal diffusivities in Si (60).

4.6.2 Structure

IM in a homogeneous, amorphous NiTi ($Ni_{65}Ti_{35}$) alloy using a Hf marker has been measured at 10 K during 1.0 MeV Kr irradiation (61). The value for the mixing was $Dt/\phi F_D$ = 13 A^5/eV, which is very similar to that for a Hf marker in pure Ni (47). This experiment demonstrates that crystal structure does not strongly influence IM. It rules out the possibility, for example, that long-range focused RCS's are an important mechanism in IM. It also adds support to the hypothesis that highly mobile self-interstitials in metals are not important for defect motion in cascades as there is no evidence for such a point defect in electron-irradiated amorphous metals.

4.6.3 Thermochemical Properties

Several researchers have noted that IM in bilayer samples depends on the thermochemical properties of these layers. Westendorp et al. showed, for example, that IM in Cu-Au was much larger than in Cu-W even though the kinematics of the irradiation were the same (62). These authors noted that the Cu-Au system has complete solubility whereas Cu and W are immiscible. Cheng et al. made the more general observation that the heat of mixing for the bilayer system is an important parameter in IM (63). This is illustrated in Fig. 6 in which IM in a series of Pt and Au bilayer are shown as a function of the heat of mixing. Like the work of Westendorp et al., systems were selected to maintain similar kinematics. In one sense, it is not surprising that systems in which the atomic species have a strong mutual attractive force will tend to mix. However, the fact that the heat of mixing is important for diffusion within the lifetime of the cascade demonstrates that interaction energies <1 eV/atom are important. BC theories, on the other hand, typically terminate when the energies fall below 5 eV.

A study of IM was also carried out in three immiscible systems of Cu, Cu-Mo, Cu-Nb, and Cu-Bi (52). As shown by the backscattering spectra in Fig. 7, mixing takes place in Cu-Nb and Cu-Bi at 10 K, but not in Cu-Mo. Although their is virtually no solid solubility in any of these systems, Cu-Nb and Cu-Bi have very small heats of mixing whereas Cu-Mo has a large positive heat of mixing. (Note Cu and Mo form immiscible liquids but Cu has complete liquid miscibility with Bi and Nb.) Calculations for IM in systems which have positive heats of mixing were performed by PA using Eq. (2) (52). PA assumed that some mixing occurs during the collisional phase of the cascade. For large positive heats of mixing, D* becomes negative (see Eq. (3)) and diffusion within the spike tends to cause segregation. It was found that for an interaction energy of 5 eV/atom, complete segregation of components mixed in the collisional phase would ensue during the subsequent thermal spike. For smaller interaction energies, .5 eV/atom, only partial segregation occurs. Values of $Dt/\phi F_D$ are 90, 7, and 2 A^5/eV for Cu- Bi, Nb, and Mo respectively. The larger value for Cu-Bi than for Cu-Nb, despite the more positive heat of mixing in the Cu-Bi system, is presumably due to the different physical properties of the systems. Bi has a high atomic mass (209) and a very low cohesive energy.

5 TEMPERATURE DEPENDENCE

The temperature dependence of IM in several metal marker systems has been investigated between 6 K and 300 K. Generally, no temperature dependence is observed between 6 K and 80 K (3). As self interstitials become mobile below 80 K in several of these metals, it shows that self-interstitial migration at low temperatures is not an important mechanism in IM. This result is not unexpectant. As most point defects undergo recombination or clustering reactions within the lifetime of the thermal spike, few isolated self-interstitials are free to migrate above stage I. Moreover, the high concentration of defect clusters produced during high dose IM experiments and which serve as interstitial traps prevents long-range migration of those few interstitials that do

remain. Isochronal annealing experiments have indeed shown that stage I recovery can be almost completely suppressed for cascade producing irradiations at high doses (64). An interesting exception to this temperature dependence was reported for a Au marker in Fe (65). An increase in IM of the order of 30-50% was observed at ~25 K. One can presently only guess at the cause of this effect, however, as free migration of interstitials occurs above 100 K in Fe, it would seem that the effect is associated with the defect structure which develops in Fe at high dose levels. For example, Kirk and Robertson have observed the formation of vacancy dislocation loops in Fe at 10 K after high-dose irradiation (66). Associating diffusion with the agglomeration of vacancies, suggests IM may be increased above 25 K in Fe due to a change in the stability of the defect structure.

Between 80 and ~300 K, a small increase, usually less than a factor of 2, is often observed (3). In Al (67) and Cu (52), for example, less than a 30% increase in IM was observed between 6 and 300 K, even though interstitials and vacancies are mobile in these metals at room temperature. The small increases in IM in metals at 300 K are probably due to the mobility of vacancies; however, until temperatures are attained in which the concentration of defect clusters can be reduced, no large increases in IM are likely to occur. Measurements above room temperature are limited in marker systems. One of the problems in using metal marker specimens above room temperature is that grain boundary diffusion becomes important and masks IM. Macht and Naundorf have overcome this problem by using markers in a specially prepared single crystal specimen (68). The results at higher temperatures require a rather complicated analysis involving point defect interactions, and the build-up and dissociation of defect clusters. These reactions are discussed in ref. (69).

The temperature dependence in bilayers have similar behavior; at low temperature there is little effect of specimen temperature, and above room temperature it grows stronger. In Fig. 7b, results for IM in the immiscible Cu-Nb and Cu-Bi systems

are illustrated (52). Clearly the IM is much reduced for the higher temperature irradiation. This result can be explained by assuming that some radiation-enhanced diffusion occurs at 300 K. Since these systems have no solid solubility, diffusion after the spike results in segregation. This can also be viewed from Eq. (3). During the spike, the temperature is high so the Darken term (1-2ΔH/kT) is positive even though ΔH is positive. Point defect motion after the spike occurs at relatively low temperatures so that 2ΔH/kT becomes large and the effective diffusion coefficient becomes negative.

The temperature dependence in silicides has been studied for some time (1). Figure 8a shows the temperature dependence of IM in Nb-Si. The apparent activation enthalpy for the diffusion coefficient is ≃0.9 eV, indicating a vacancy migration enthalpy of 1.8 eV (70). To illustrate that this temperature dependence can be associated with point defect mobility, the effect of dose-rate on IM was measured. According to RED theory, diffusion occurring within individual cascades should be independent of both temperature and dose-rate. For diffusion limited by point defect recombination, the width of the mixed layer should depend on temperature and dose rate according to, (41)

$$\langle x^2 \rangle^{1/2} \propto \dot{\phi}^{-1/4} \cdot \exp(-E_{mv}/4kT) \cdot \phi^{1/2} \qquad (7)$$

Figure 8b shows the effect of dose rate at 295 K and 320 K (71). At 295 K, no apparent temperature dependence was observed, nor correspondingly, a dose-rate dependence. At 325 C, IM becomes both temperature and dose rate dependence. For the change in dose rate of a factor of 20, the predicted change in width is a factor ≃2; the experiment showed a factor of ~1.6.

From these results, it appears that RED plays only a small role in IM at temperatures below those corresponding to those of stage V, even though vacancies and interstitials become mobile well below these temperatures. This is due to the build-up of a defect structure which serves as sinks for the mobile defects. Until this defect

structure dissolves in stage V, the increase in IM due to RED is greatly restricted. On the other hand, a small amount of diffusion by defects above stages I and III may be very important in suppressing mixing in systems like Cu-Bi or Cu-Nb which have little solid solubility. It is also important for determining the structures of irradiated alloys or ion-beam mixed materials since small rearrangements of atoms can be very important in such processes as short range ordering or amorphization.

6 CONCLUSIONS

A qualitative understanding of the fundamental processes of IM in metals has now been achieved based on standard radiation damage theory. It was deduced from investigating the influences of physical and thermochemical properties of the targets, the type of irradiation particle, and temperature, that IM at low temperatures is dominated by diffusion during the thermal spike phase of the cascade and that it can be reasonably modeled by RED theory. The collisional phase of the cascade appears to be important mostly for establishing the initial conditions of the spike. This result has the implication for materials modification applications that the characteristic energy for atomic rearrangement processes during low-temperature irradiation is <1 eV, and not >5 eV which is typical of displacement processes. This has importance for structure and short range ordering effects since interaction energies between different atoms can be higher than 1 eV/atom. The inability to mix immiscible systems such as Cu-W or Cu-Mo, even at liquid helium temperatures, illustrates this point. At higher temperatures, RED tends to move the system toward lower energy thermodynamic states. As characteristic energies of defect motion during this diffusion process are less than tenths of eV's, an understanding of RED requires a detailed knowledge of point defect mobilities and interactions.

In semiconductor systems, the understanding of IM parallels that of other radiation effects. Generally, they are more complicated, and not well known, and this

makes it difficult to assess the results for IM. For example, the linear dependence of the mixed layer on dose and stoichiometric composition profiles can not be easily interpreted without knowing the point defect mobilities in these systems.

ACKNOWLEDGMENTS

The author wishes to acknowledge many enlightening discussions with Prof. David N. Seidman and his colleagues at Caltech and at ANL.

REFERENCES

1. J.W. Mayer, B.Y. Tsaur, S.S. Lau, and L.S. Hung, Nucl. Instr. and Meth. 182/183 (1981) 1.

2. M-A. Nicolet, T.C. Banwell, and B.M. Paine, MRS Symp. Proc. Vol. 27 (Elsevier, New York, 1984) 3.

3. B.M. Paine and R.S. Averback, Nucl. Instr. and Meth. B7/8 (1985) 666.

4. W.L. Johnson, Y.T. Cheng, M. Van Rossum, and M-A. Nicolet, Nucl. Instr. and Meth., B7/8 (1985) 657.

5. Z.L. Wang, J.F.M. Westendorp, and F.W. Saris, Nucl. Instr. and Meth. 209/210 (1983) 115.

6. J.R. Beeler, Jr. and M.F. Beeler, in *Fundamental Aspects of Radiation Damage in Metals*, CONF-751006-P1 (1976) 28.

7. J.B. Gibson, A.N. Goland, M. Milgram, and G.H. Vineyard, Phys. Rev. 120 (1960) 1229.

8. *M.A. Kirk and T.H. Blewitt, Met. Trans. 9A (1978) 1729.*

9. P. Sigmund, Rev. Roumaine Phys., 17 (1972) 823, 969, 1079.

10. W.E. King and R. Benedek, J. Nucl. Mater. 117 (1983) 26.

11. M.W. Guinan and J.H. Kinney, J. Nucl. Mater. 103/104 (1981).

12. M.T. Robinson and I.M. Torrens, Phys. Rev. B9 (1974) 5008.

13. J.R. Beeler, Jr., Phys. Rev. 150 (1966) 470.

14. H.J. Wollenberger, in *Vacancies and Interstitials in Metals*, ed. A. Seeger et al. (North Holland, Amsterdam, 1970) p. 215.

15. P. Sigmund, Radiat. Eff. 1, (1969) 15.

16. P. Sigmund and A. Gras-Marti, Nucl. Instr. and Meth. 182/182, (1981) 25.

17. U. Littmark, Nucl. Instr. and Meth. B7/8 (1985).

18. S. Matteson, B.M. Paine, and M-A. Nicolet, Nucl. Instr. and Meth. 182/183 (1981) 53.

19. W. Möller and W. Eckstein, Nucl. Instr. and Meth. B7/8 (1985).

20. F.-Z. Cui and H.D. Li, Nucl. Instr. and Meth. B7/8 (1985) 650.

21. J.P. Biersack and L.G. Haggmark, Nucl. Instr. and Meth. 174 (1980) 257.

22. F. Seitz and J. Koehler, Sol. Stat. Phys., Vol. 2, ed. F. Seitz and D. Turnbull (Academic Press, New York, 1956).

23. D. Peak and R.S. Averback, Nucl. Instr. and Meth. B7/8 (1985).

24. K.B. Winterbon, *Ion Implantation and Energy Deposition Distributions*, Vol. 2 (Plenum Press, 1975, New York).

25. W.M. Lomer, AERE Report T/R 1540 (1954).

26. W. Schilling, G. Burger, K. Isebeck, and H. Wenzl, in Ref. 13, p. 255.

27. R.S. Averback, R. Benedek, and K.L. Merkle, Phys. Rev. B18 (1978) 4156.

28. R.S. Averback, R. Benedek, K.L. Merkle, and J. Sprinkle. J. Nucl Mater. 113 (1983) 211.

29. C. Jaoruen, J.P. Riviere, C. Templier and J. Delafond, J. Nucl. Mater. 131 (1985) 11.

30. P. Jung, J. Nucl. Mater. 117 (1983) 70.

31. M.W. Guinan, private communication.

32. Ching-Yeu Wei, Michael I. Current, and David N. Seidman, Phil. Mag., A44 (1981) 459.

33. E.M. Schulson, J. Nucl. Mater. 83 (1979) 239.

34. C. English, B.L. Eyre, A.F. Barlett, H.N.G. Wadley, Phil Mag. 35 (1977) 533.

35. K. Haga, A.C. Baily, W.E. King, K.L. Merkle, and M. Meshi, 7th Int. Conf. of High Voltage Electron Microscopy, eds. R.M. Fisher, R. Gronsky, and K.H. Westmacott (1983) p. 139.

36. K.L. Merkle and W.E. King, unpublished.

37. T.J. Black. M.L. Jenkins, and M.A. Kirk, Proc. EMAG 83, ed. P. Doig, Inst. of Phys. Series No. 68, London 1984, p. 343.

38. Dipankar Pramanik and David N. Seidman, J. Appl. Phys. 54 (1983) 6352.

39. J.F.M. Westendorp, P.K. Rol, J.B. Sanders, and F.W. Saris, Nucl. Instr. and Meth., B7/8 (1985) 616.

40. F. Besenbacher, J. Bottinger, S.K. Nielsen, and H.J. Whitlow, Appl. Phys. A 29 (1982) 141.

41. R.S. Averback, L.J. Thompson, Jr., J. Moyle, and M. Shalit, J. Appl. Phys. 53 (1982) 1342.

42. B.R. Appleton, in *Ion Implantation and Beam Processing*, ed. J.S. Williams and J.M. Poate (Academic Press, New York, 1984) p. 189

43. D.B. Poker, 2nd Workshop on Ion Beam Mixing, Pasadena Ca. (1985).

44. D.B. Poker, unpublished.

45. U. Shreter, Frank C.T. So, and M-A. Nicolet, J. Appl. Phys. 55 (1984) 3500.

46. S. Matteson, B.M. Paine, M.G. Grimaldi, G. Mezey, and M-A. Nicolet, Nucl. Instr. and Meth. 182/182 (1981) 43.

47. R.S. Averback and D. Peak, Appl. Phys. A. in press.

48. R.S. Averback, L.J. Thompson, and L.E. Rehn, MRS Proc. Vol. 27 (Elsevier, 1984, New York) 25.

49. J. Bottinger, S.K. Nielsen, and P.T. Thorsen, Nucl. Instr. and Meth. B7/8 (1985) 707.

50. P. Sigmund, Appl. Phys. Lett. 25 (1974) 169, and Appl. Phys Lett. 27 (1975) 52.

51. H.H. Andersen and H.L. Bay, Radiat. Eff. 19 (1973) 139; and H.H. Andersen and H.L. Bay, J. Appl. Phys. 45 (1974) 953.

52. R.S. Averback, D. Peak, and L.J. Thompson, Appl. Phys. A. in press.

53. S.-J. Kim, R.S. Averback, D. Peak, and M-A. Nicolet, 2nd Workshop on Ion Beam Mixing, Pasadena, Ca. 1985.

54. M. Van Rossum, Y.-T. Cheng, W.L. Johnson, and M-A. Nicolet, Appl. Phys. Lett. 1984.

55. H.H. Andersen, Appl. Phys. 18, 131.

56. P. Lucasson, Ref. 6, p. 42.

57. This is deduced from the Van Liempt relation.

58. M.W. Finis, unpublished.

59. D. Peak, 2nd Workshop on Ion Beam Mixing, Pasadena Ca. 1985.

60. A.J. Barcz, B.M. Paine, and M-A. Nicolet, Appl. Phys. Lett. 44 (1984) 45.

61. H. Hahn, R.S. Averback, T. de la Rubia, and P.R. Okamoto, unpublished.

62. H. Westendorp, Zhong-Lie Wang, and F.W. Saris, Nucl. Instr. and Meth. 194 (1982) 453.

63. Y.-T. Cheng, M. Van Rossum, M-A. Nicolet , and W.L. Johnson, Appl. Phys. Lett. 45 (1984) 185.

64. R.S. Averback, L.J. Thompson, and K.L. Merkle, J. Nucl Mater. 69/70 (1978) 714.

65. J. Bottinger, S.K. Nielsen, H.J. Whitlow, and P. Wriedt, Nucl. Instr. and Meth. 218 (1983) 684.

66. M.A. Kirk and I. Robertson, MRS Proc. 1985 in press.

67. S. Mantl, L.E. Rehn, R.S. Averback, and L.J. Thompson, Nucl. Instr. and Meth., B7/8 (1985) 622.

68. M.-P. Macht and V. Naundorf, J. Appl. Phys. 53 (1982) 7551.

69. A.D. Brailsford and R. Bullough, J. Nucl. Mater. 60/70, (1978) 434.

70. S. Matteson, J. Roth, and M-A. Nicolet, Radiat. Eff. 42 (1979) 217.

71. R.S. Averback, T. Banwell, and M-A. Nicolet, unpublished.

72. R.H. Zee, M.W. Guinan and G.L. Kulcinski, J. Nucl Mater., 114 (1983) 190.

73. M.W. Guinan, J.H. Kinney, R.A. van Konynenburg, and A.C. Damask, unpublished result.

74. D. Becker, et al. Phys. Status Solidi 30 (1968) 219.

75. J.P. Riviere and J.F. Dinhut, J. Nucl. Mater. 118 (1983) 333.

TABLE 1 Ratio of replacements per displacement for fast neutron and electron irradiation in selected alloy systems

System	Fast Neutrons	Electrons	Ref.
CuPd	24	3.1	72
Ni_3 Mn	16[a]	2.2[b]	a)8, b)74
Cu_3 Au	50	-	8, 73
FeCo	90	32	75

TABLE 2 Predicted values of IM in various hosts (Ref. 59)

			$\langle\Delta x^2\rangle/2\Phi_D(Å^5/eV)$	
Host	Evm(eV)	$D_o(Å^2s^{-1})$	Predicted[a]	Measured[b]
Ag	0.65	1.6×10^{15}	56	60-90
Al	0.61	8×10^{14}	24	20-40
Au	0.82	1.4×10^{14}	70	80-140
Cu	0.69	6×10^{14}	19	20-26
Fe	1.17	3×10^{14}	2	6-7
Mo	1.30	2×10^{15}	16	6
Ni	1.39	8×10^{14}	6	8-10
Pt	1.39	1×10^{14}	24	16-24
W	1.69	7×10^{13}	11	6-15

[a]Efficiencies calculated by PA assuming E_{mv}(spike) = 1/3 E_{mv}(thermal).

[b]Values reported by Kim et al. (53).

FIGURE CAPTIONS

FIGURE 1 Pictoral representation of the primary recoil spectrum for a 100 keV cascade in fcc Fe derived from binary collision computer simulation and showing distinct subcascade formation (Beeler et al. 6)

FIGURE 2 Time evolution of a 2.5 keV cascade in W simulated using molecular dynamics. Three distinct phases are apparent; the initial displacement phase in which many atoms are displaced from their lattice sites, a relaxation phase in which close FP's spontaneously recombine, and a "thermal spike" phase in which stimulated motion of point defects induces additional recombination and IM

FIGURE 3 The ratio of the number of defects produced in a cascade to that calculated by the Kinchin-Pease model as a function of recoil energy. Ratio determined from: (o), experimental (28); and binary collision (x) or molecular dynamics (+) computer simulation. MD results pertain to W.

FIGURE 4 The value of $Dt/\phi \cdot F_D$ in marker (49) and bilayer (50) samples for different types of projectile irradiations

FIGURE 5 The value of $Dt/\phi \cdot F_D$ (53) for many metal marker systems for 0.5-1.0 MeV Kr irradiation at 6 K. Circles representing each host is located by its cohesive energy (abscissa) and the energy density along the track of the projectile (ordinate)

FIGURE 6 Values of IM as a function of the heat of mixing for a series of Au and Pt bilayer samples. (from Ref. 63)

FIGURE 7 Backscattering spectra illustrating IM in Cu-Mo, Cu-Nb and Cu-Bi at 6 and 295 K. The spectra for the irradiated specimens (dotted lines) are shifted on abscissa to better reveal mixing. The ion doses were 2.1,2.1, and 0.57 ions/$Å^2$ for the three systems respectively (from ref. 52)

FIGURE 8 a) Temperature dependence of IM in Nb-Si (from Ref. 70); b) Effect of dose-rate on IM in the same Nb-Si system as in (a).

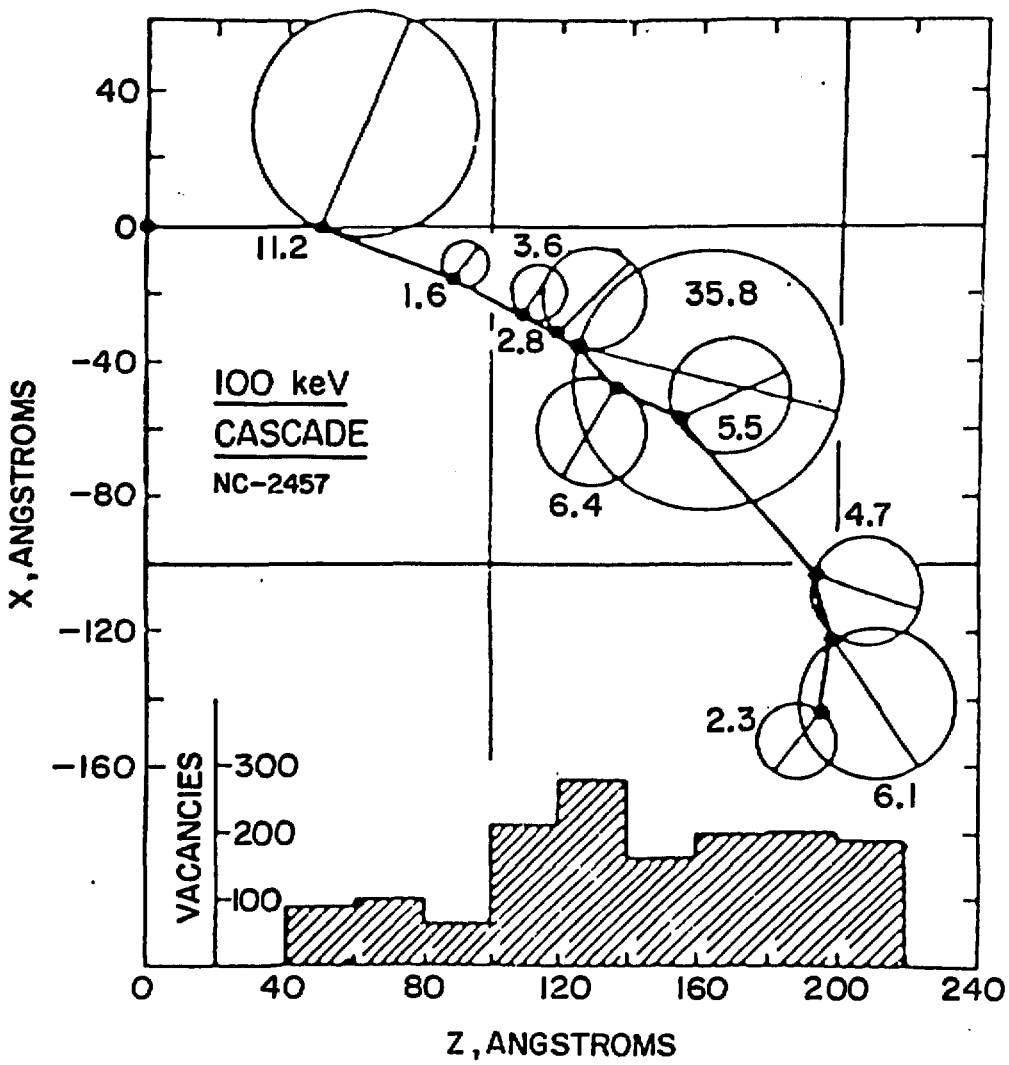
40
0
-40
-80
-120
-160
X, ANGSTROMS
11.2
1.6
3.6
2.8
35.8
5.5
6.4
4.7
2.3
6.1
100 keV
CASCADE
NC-2457
VACANCIES
300
200
100
0
40
80
120
160
200
240
Z, ANGSTROMS

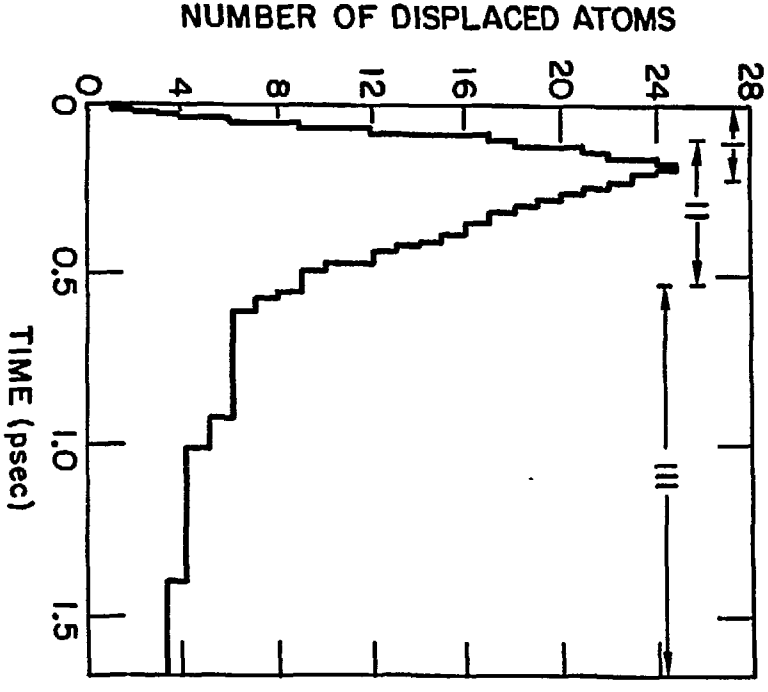
NUMBER OF DISPLACED ATOMS
0
4
8
12
16
20
24
28
TIME (psec)
0
0.5
1.0
1.5
I
II
III

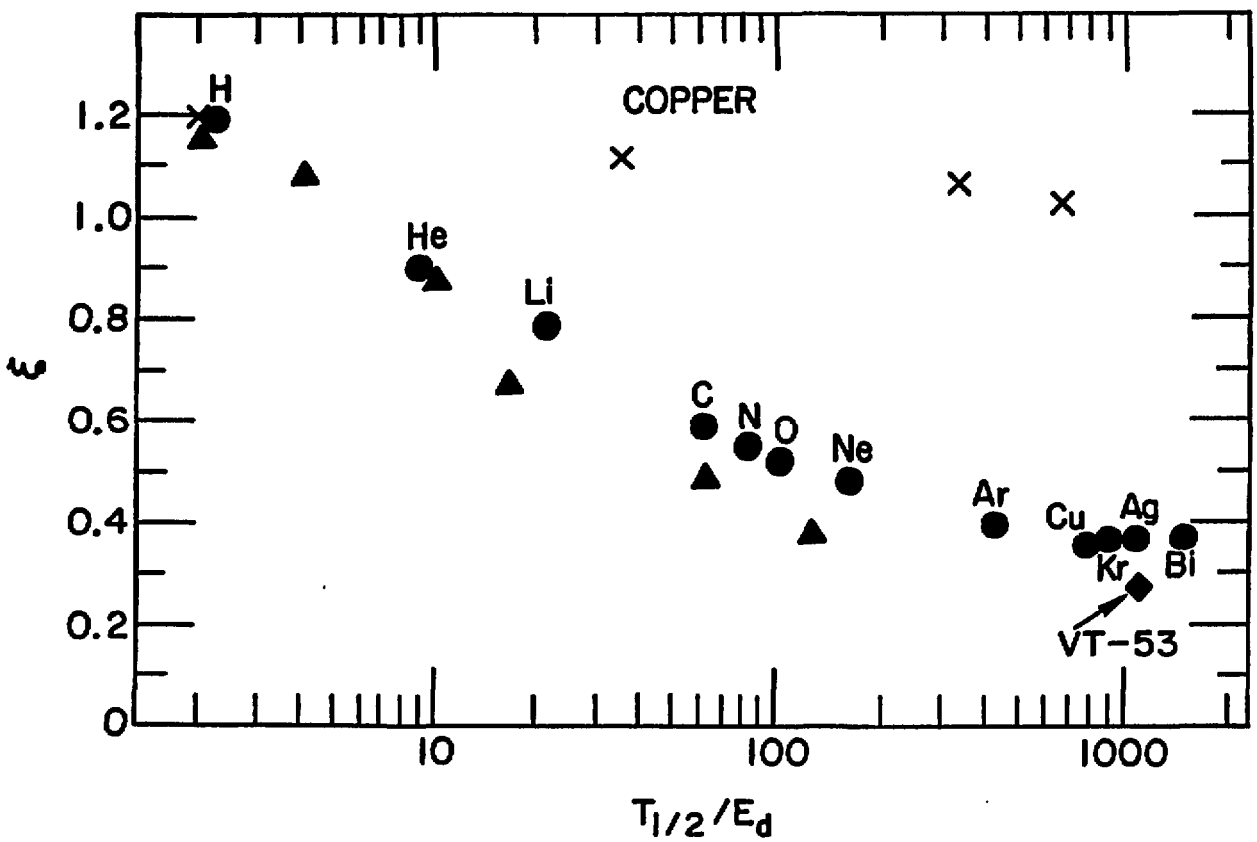
COPPER
H
He
Li
C
N
O
Ne
Ar
Cu
Ag
Kr
Bi
VT-53
1.2
1.0
0.8
0.6
0.4
0.2
0
10
100
1000
$T_{1/2}/E_d$

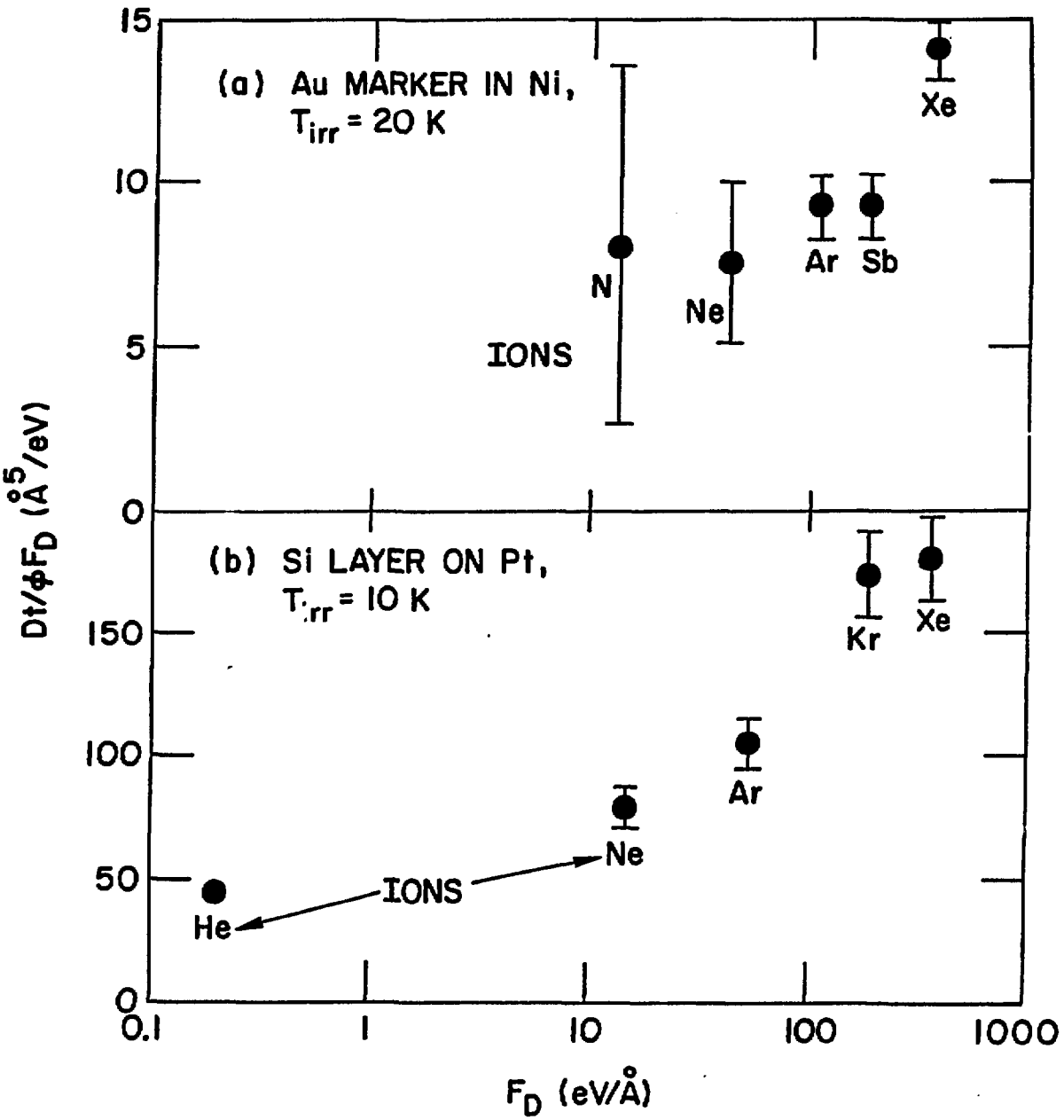
(a) Au MARKER IN Ni,
T_{irr} = 20 K
IONS
N
Ne
Ar
Sb
Xe
(b) Si LAYER ON Pt,
T_{irr} = 10 K
He
IONS
Ne
Ar
Kr
Xe
15
10
5
0
150
100
50
0
0.1
1
10
100
1000
$Dt/\phi F_D$ (Å^5/eV)
F_D (eV/Å)

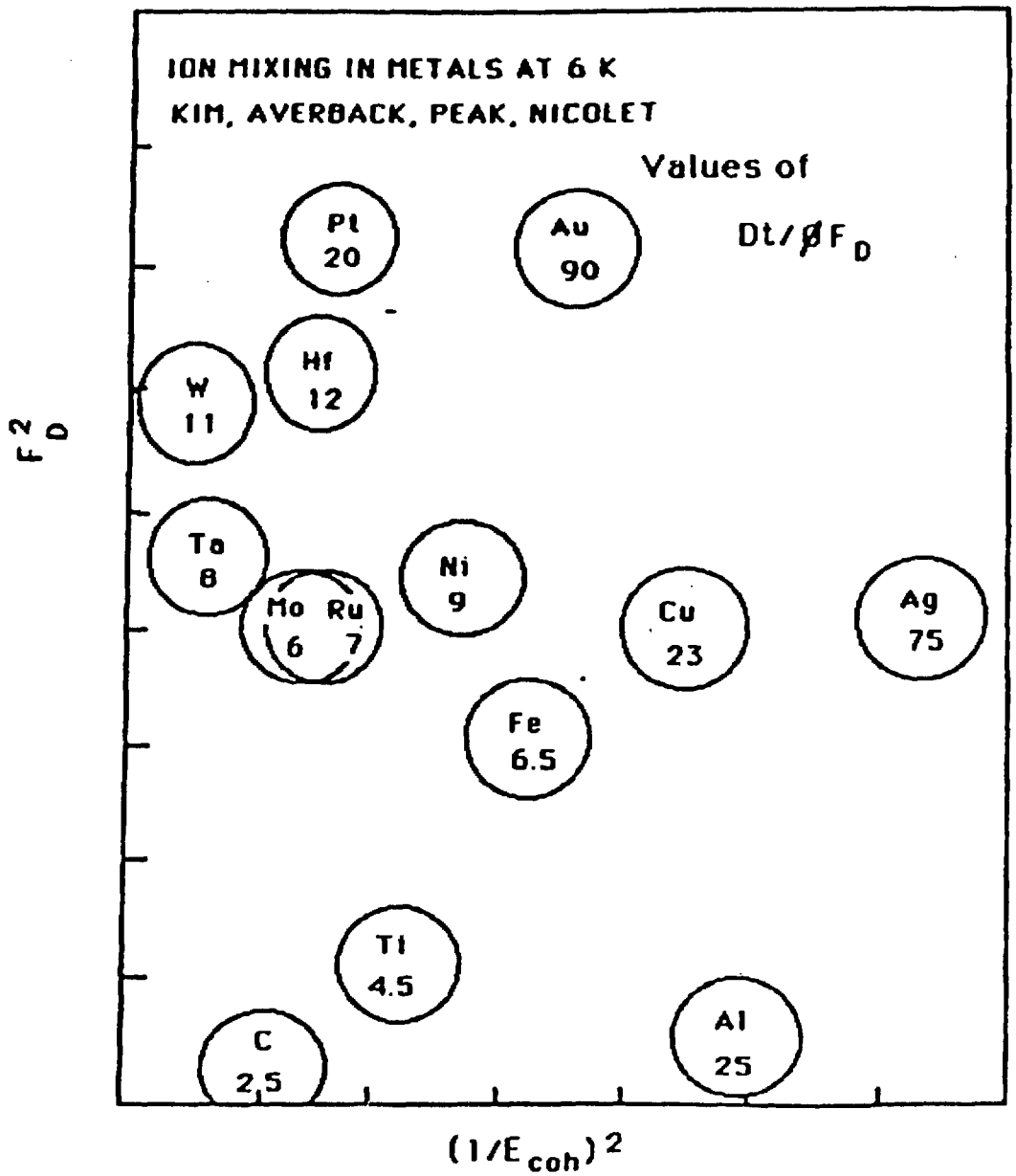
ION MIXING IN METALS AT 6 K
KIM, AVERBACK, PEAK, NICOLET
Values of
$Dt/\phi F_D$
Pt 20
Au 90
Hf 12
W 11
Ta 8
Mo 6
Ru 7
Ni 9
Cu 23
Ag 75
Fe 6.5
Ti 4.5
C 2.5
Al 25
F_D^2
$(1/E_{coh})^2$

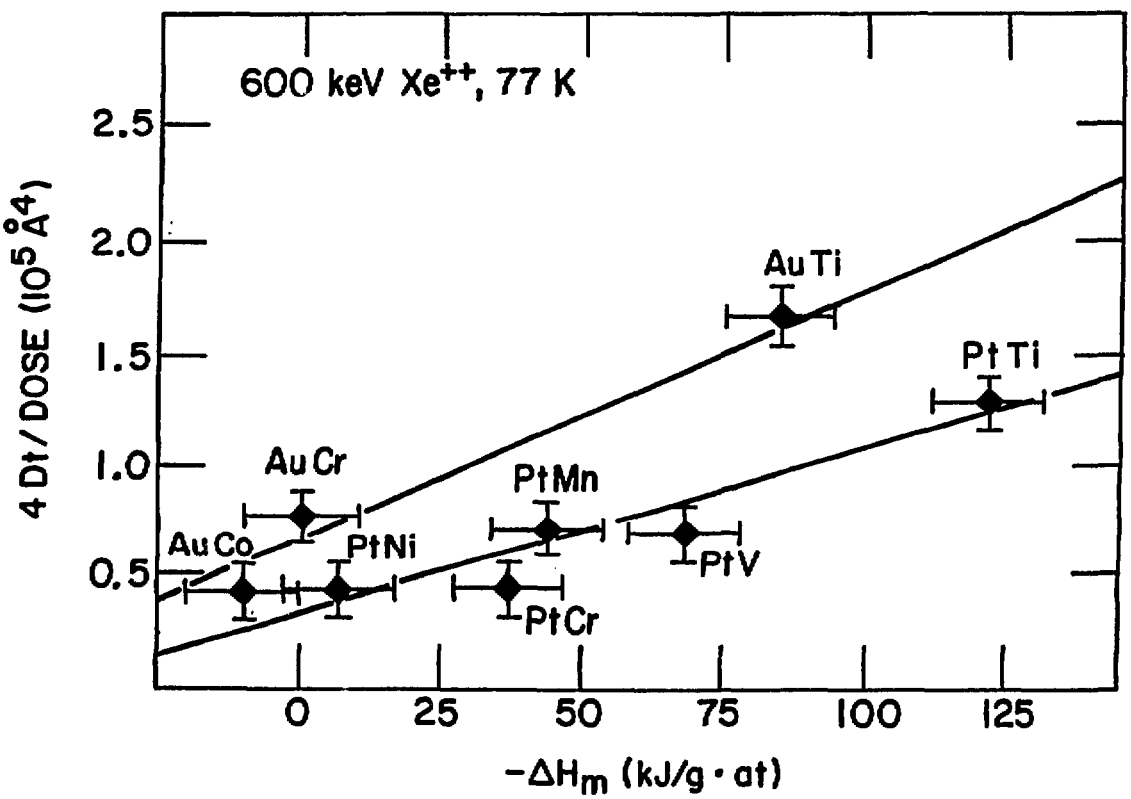
600 keV Xe++, 77 K
4 Dt / DOSE (10^5 Å^4)
2.5
2.0
1.5
1.0
0.5
0
25
50
75
100
125
-ΔHm (kJ/g • at)
Au Ti
Pt Ti
Au Cr
Pt Mn
Au Co
Pt Ni
Pt V
Pt Cr

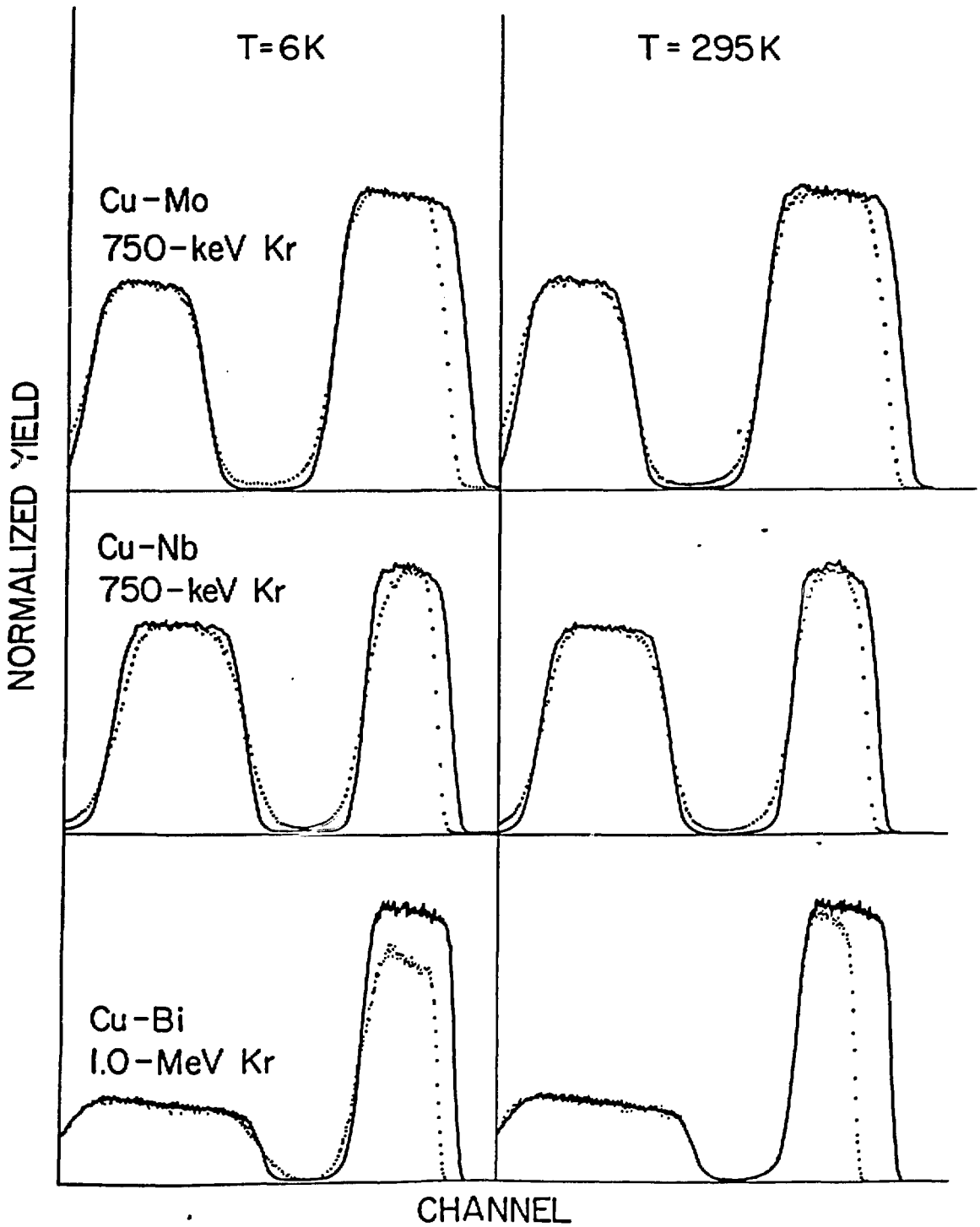
T=6K
T=295K
Cu-Mo
750-keV Kr
Cu-Nb
750-keV Kr
Cu-Bi
1.0-MeV Kr
NORMALIZED YIELD
CHANNEL

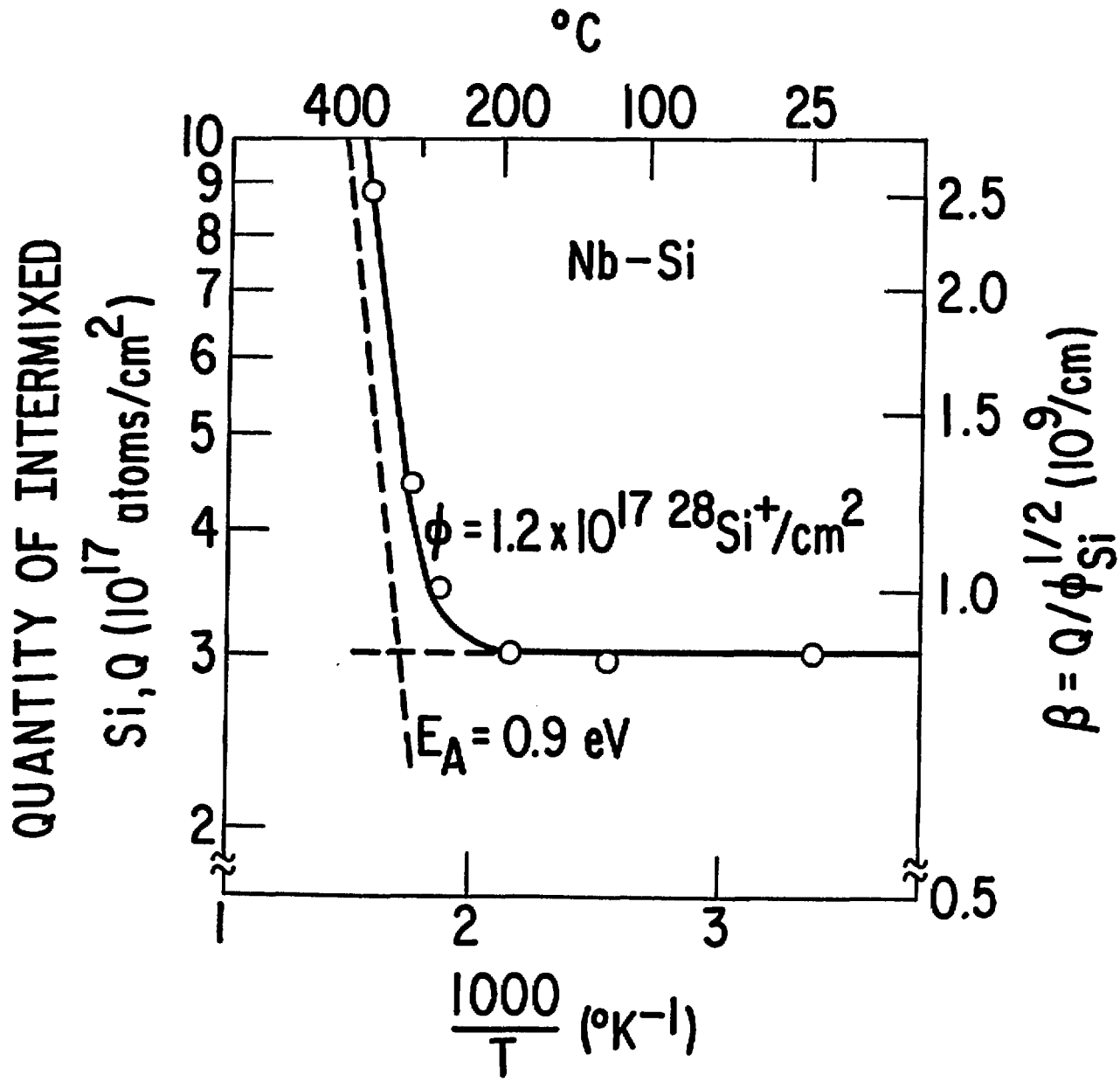
°C
400
200
100
25
10
9
8
7
6
5
4
3
2
Nb-Si
$\phi = 1.2 \times 10^{17}\ ^{28}Si^{+}/cm^{2}$
$E_A = 0.9$ eV
2.5
2.0
1.5
1.0
0.5
1
2
3
$\frac{1000}{T}$ (°K⁻¹)
QUANTITY OF INTERMIXED Si, Q (10^{17} atoms/cm^2)
$\beta = Q/\phi_{Si}^{1/2}$ (10^9/cm)

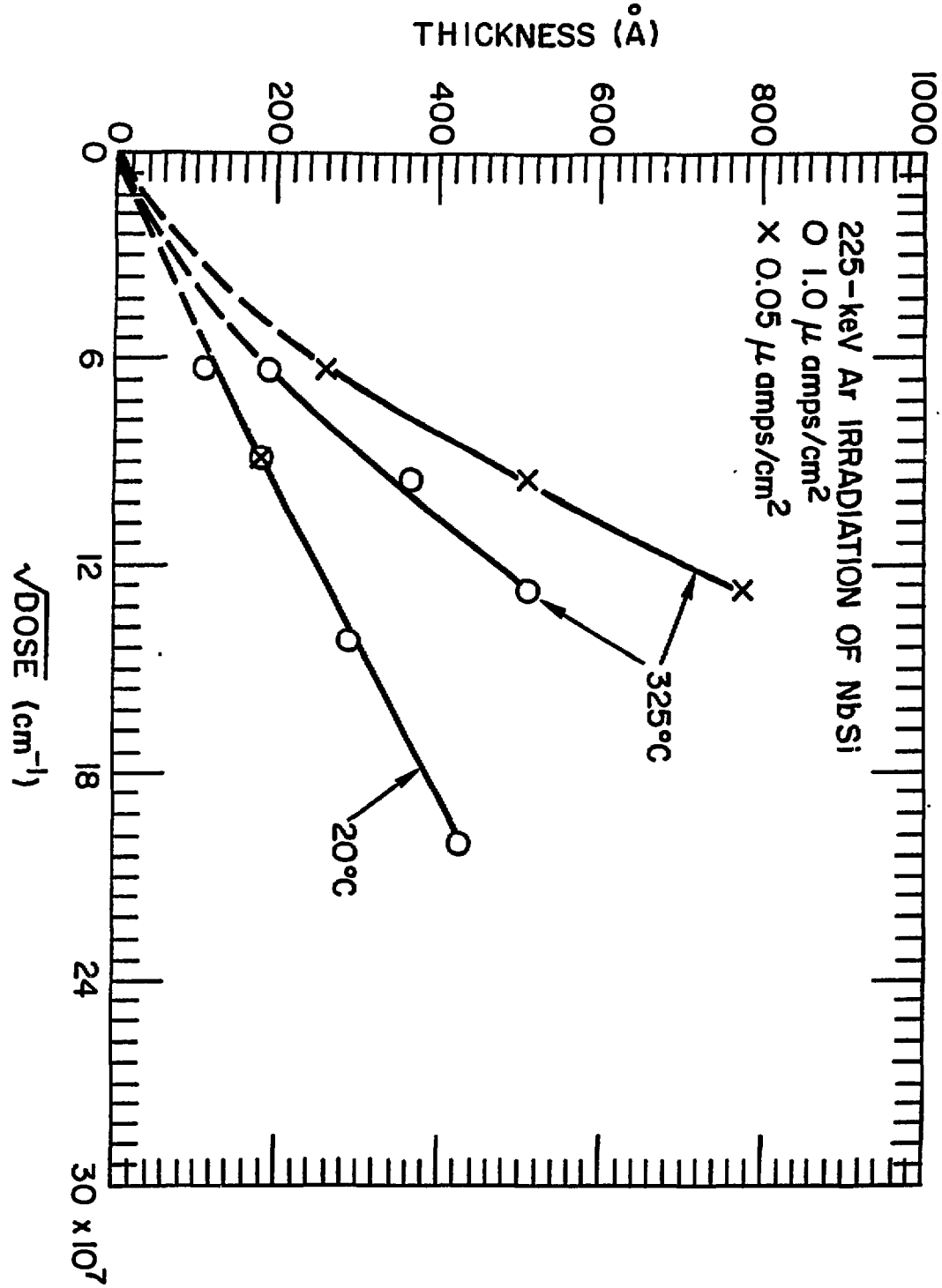
THICKNESS (Å)
0
200
400
600
800
1000
225-keV Ar IRRADIATION OF NbSi
O 1.0 μ amps/cm²
× 0.05 μ amps/cm²
325°C
20°C
0
6
12
18
24
30 × 10⁷
√DOSE (cm⁻¹)